Journal of Atmospheric and Solar–Terrestrial Physics 208 (2020) 105376

Contents lists available at ScienceDirect

Journal of Atmospheric and Solar-Terrestrial Physics

journal homepage: www.elsevier.com/locate/jastp

Research Paper

A survey of geomagnetic and plasma time lags in the solar-wind-driven magnetosphere of earth

Joseph E. Borovsky

Space Science Institute, Boulder, CO, USA

ARTICLE INFO

Keywords:
Magnetosphere
Solar wind
Geomagnetic activity
Plasma

ABSTRACT

Sixteen variables describing the state of the magnetosphere are examined in the years 1991–2007; the sixteen variables include nine geomagnetic indices plus seven measures of electron and ion precipitation into the atmosphere, the rate of substorm occurrence, the pressure and number density of the ion plasma sheet, the flux of substorm-injected electrons, and the radiation-belt electron flux. Eight other variables are used to represent the properties of the solar wind at Earth. To estimate the time lags between magnetospheric and solar-wind variables bivariate (two-variable) linear correlations, multivariate linear correlations, and vector-vector correlations are utilized. Using bivariate correlation the lag time of each magnetospheric variable with respect to each solar-wind variable is varied to obtain the maximum correlation coefficient. Using multivariate linear correlations, the time series of each magnetospheric variable is correlated with a linear combination of the eight time series of the eight solar-wind variables, with eight independent lead times on the eight solar-wind variables optimized to produce the largest multivariate correlation coefficient. The resulting time lag between each magnetospheric variable and each solar-wind variable is then catalogued. Additionally, the solar-wind variables that most-strongly affect each of the 16 magnetospheric variables are noted. A similar process of optimizing lag times on magnetospheric variables is performed during vector-vector correlations between a 9-dimensional magnetospheric state vector and an 8-dimensional solar-wind state vector.

1. Introduction

There are multiple time lags in the reaction of the magnetosphere to changes in the solar wind (Borovsky and Valdivia, 2018), from minutes (the reaction to changes in the solar-wind dynamic pressure) to a few days (e.g. the evolution of the outer electron radiation belt during sustained solar-wind driving or the filling of the outer plasmasphere after solar-wind driving is reduced). It is well known that magnetospheric activity as measured by geomagnetic indices lags the solar wind by timescales from minutes to hours (e.g. Arnoldy, 1971; Iyemori et al., 1979; Smith et al., 1999; Newell et al., 2007). Magnetospheric particle populations also lag the properties of the solar-wind plasma; these include the ion plasma sheet and the electron plasma sheet with time lags of hours (Borovsky et al., 1998; Denton and Borovsky, 2009), the population of substorm-injected electrons in the dipole with time lags of hours (Borovsky and Yakymenko, 2017), and the outer electron radiation belt with times lags of hours and days (Balikhin et al., 2011; Wing et al., 2016; Borovsky, 2017). Most often these time lags are determined by optimizing correlation coefficients between a single magnetospheric variable and a single solar-wind "driver function".

In this report a brief survey of magnetospheric time lags is performed using optimization of correlation. The differences here from past calculations are the use of (a) multivariate correlations and (b) vector-vector correlations. Multivariate correlations between a single magnetospheric variable and multiple solar-wind variables produce higher correlation coefficients than do correlations between a single magnetospheric variable and either a single solar-wind variable or a single solar-wind function (Borovsky and Denton, 2018). Vector-vector correlations produce even higher correlation coefficients (Borovsky and Osmane, 2019).

This report is organized as follows. In Section 2 the 1-hr resolution data sets for solar-wind variables and magnetospheric variables in the years 1991–2007 are described, as are the multivariate-correlation methods and the vector-vector correlation methods. Section 3 describes the results (1) of bivariate (two-variable) correlations between a single magnetospheric variable and a single solar-wind variable and (2) of multivariate correlations with a single magnetospheric variable and a set of eight solar-wind variables. In Section 4 the results of correlations

E-mail address: jborovsky@spacescience.org.

https://doi.org/10.1016/j.jastp.2020.105376
Received 2 December 2019; Received in revised form 10 June 2020; Accepted 19 June 2020
Available online 26 June 2020

between a solar-wind state vector and a magnetospheric state vector with multiple optimized time lags are described. Section 5 summarizes the results, discusses the interpretation of the time lags, and suggests future work.

2. Methods and data sets

The set of magnetospheric variables explored are listed in Table 1. The first nine variables are commonly used geomagnetic indices. A variety of geomagnetic indices have been chosen: the auroral electrojet indices AE, AL, and AU (Davis and Sugiura, 1966), the polar-cap index PCI (Troshichev et al., 1988), the magnetospheric convection indices Kp and am (Thomsen, 2004), and the plasma diamagnetic indices Dst, SYMH, and ASYM (Katus and Liemohn, 2013). The 10th variable in Table 1 S_{rate} is the rate of substorm occurrence, which is defined as $S_{rate} = \log_{10}(24/\Delta t)$, with Δt being the time between substorm onsets (the previous onset in time to the next substorm that occurs in the data set) in units of hr (Borovsky and Yakymenko, 2017); the substorm occurrence rate in units of substorms per day is 10 to the power S_{rate} and S_{rate} is evaluated at the midpoint of every hour of universal time. The two variables mP_e and mP_i are the DMSP-spacecraft estimates of the northern and southern hemispheric power in electron precipitation (mP_e) and ion precipitation (mP_i) in units of GW (Emery et al., 2008, 2009). P_{ips} is a multispacecraft average of the pressure of the ion plasma sheet around geosynchronous orbit (Borovsky, 2017) and n_{ips} is a multispacecraft average of the number density of the ion plasma sheet around geosynchronous orbit (Borovsky, 2017). The quantity F_{e130} is the logarithm of the peak flux of 130-keV substorm-injected electrons at geosynchronous orbit as measured by multiple spacecraft (Borovsky and Yakymenko, 2017). The variable $F_{el.2}$ is a multispacecraft average of the outer-radiation-belt electron-flux index at 1.2 MeV (Borovsky and Yakymenko, 2017). The final column of Table 1 describes the functional form of each magnetospheric variable that is used in the correlative studies. Variables that have very non-Gaussian occurrence distributions are put into logarithms to make their occurrence distributions more Gaussian like.

The eight variables that are used to represent the solar wind are (1) the solar-wind speed $v\sigma w$ (in the functional form $\log_{10}(v\sigma w)$), (2) the proton number density n_{sw} (in the functional form $\log_{10}(n\sigma w)$), (3) the 10.7-cm radio flux of the Sun F10.7 (in the functional form $\log_{10}(F10.7)$), (4) the GSM Z-component magnetic field B_z (in the form $-B_z$), (5) a Mach-number function $f(M_A) = M_A^{-1.35}(1 + 680M_A^{-3.30})^{-1/4}$ (cf. eq. (3b) of Borovsky and Yakymenko, 2017) that represents the compression ratio of the bow shock and the plasma beta of the magnetosheath, where $M_A = v_{sw}/v_A$ is the Alfven Mach number of the solar wind, (6) the GSM clock angle $\theta_{clock} = \mathrm{Arccos}(B_z/(B_y^2+B_z^2)^{1/2})$ of the magnetic field (in the functional form $\sin^2(\theta_{clock}/2)$), (7) the angle between the solar-wind magnetic-field vector and the Earth-Sun line θ_{Bn} (in the functional form θ_{Bn}), and (8) the normalized fluctuation amplitude of the magnetic field $\Delta B/B_{mag}$ (in the form $0.1 + \Delta B/B_{mag}$), where ΔB is the rms variance of the vector $\underline{\mathbf{B}}$ during 1 h of data and $B_{mag} = (B_x^2+B_y^2+B_z^2)^{1/2}$ is the average magnetic-field strength during that hour. $\Delta B/B_{mag}$ is the angular wiggle (in radians) of the solar-wind magnetic-field direction vector.

For the magnetospheric variables and the solar-wind variables, hourly values are used for the years 1991–2007. The solar-wind variables come from the OMNI2 hourly data set of measured upstream values advected to the nose of the magnetosphere (King and Papitashvili, 2005; Weimer and King, 2008). If an hour does not contain a data value for each of the 16 magnetospheric variables and for each of the 8 solar-wind variables, that hour is not included in any of the correlations. In the 1991–2007 data set there are 102,674 complete hours. For N = 102,674 data points random correlations are expected to have a Pearson linear correlation coefficient $|R_{corr}| < 2/(N+1)^{1/2} = 0.006$ (e.g. Beyer, 1966; Bendat and Piersol, 1971): because of the strong intercorrelations between solar-wind variables (e.g. Borovsky, 2018), correlation coefficients between solar-wind variables and magnetospheric variables will rarely be this small. The standard error S_{err} (uncertainty) in the correlation coefficient R_{corr} for N data points is $S_{err} = (1\text{-}R_{corr}^2)^{1/2}/(N\text{-}2)^{1/2}$: whatever the value of the correlation coefficient R_{corr}, the standard error for N = 102,674 points is $S_{err} = 0.003$ or less.

Note that Kp and am have 3-hr time resolution so their hourly values repeat three times in a row; in the first of the 3 h geomagnetic information from 1 to 2 h into the future appears, in the second hour information from 1 h into the future and into the past appears, and in the third hour information from 1 to 2 h into the past appears. When examining the causality and time lags of solar-wind/magnetosphere coupling, this can produce some confusion. Higher-time-resolution versions of the Kp index are now being developed (cf. Matzka et al., 2019).

All variables are put into standardized forms where the mean value is subtracted and then the variable is divided by its standard deviation for the entire 17-year interval. For example, a variable X in a logarithmic functional form $\log_{10}(X)$ would be standardized to $(\log_{10}(X) - \langle\log_{10}(X)\rangle)/\sigma(\log_{10}(X))$ where $\langle\log_{10}(X)\rangle$ is the 17-year mean value of $\log_{10}(X)$ for the data set and $\sigma(\log_{10}(X))$ is the standard deviation of the hourly $\log_{10}(X)$ values for the 17-year entire data set. Note that standardization removes the units from a variable.

Bivariate linear correlations are performed between single magnetospheric variables and single solar-wind variables with a lead time on the solar-wind variable that is adjusted by 1-hr increments to maximize the Pearson linear correlation coefficient. With 16 magnetospheric variables and 8 solar-wind variables the bivariate correlation process is performed 128 times yielding 128 two-variable lead times.

Multivariate linear correlations are performed between each of the individual magnetospheric variables and the set of eight solar-wind variables. Representing a solar-wind variable as $s_j(t)$, the multivariate correlation yields a relation between the single magnetospheric variable m(t) and a linear combination of the eight solar-wind variables of the form

$$m(t) \leftrightarrow c_1 s_1(t+\tau_1) + c_2 s_2(t+\tau_2) + c_3 s_3(t+\tau_3) + c_4 s_4(t+\tau_4) + c_5 s_5(t+\tau_5) + c_6 s_6(t+\tau_6) + c_7 s_7(t+\tau_7) + c_8 s_8(t+\tau_8) \quad (1)$$

where the c_j are the numerical coefficients assigned to the solar-wind

Table 1
For the 16 magnetospheric variables, the Pearson linear correlation coefficient for multivariate fits between each magnetospheric variable and eight solar-wind variables are listed; the first column is the correlation coefficient with no time lags, the second column is the correlation coefficient with optimized time lags, and the final column is the functional form of the magnetospheric variable that is used in the correlations.

Magnetospheric Quantity	Multivariate R_{corr} without Time Lags	Multivariate R_{corr} with Time Lags	Functional Form Used in Correlations
AE	0.7806	0.8418	$\log_{10}(1+AE)$
AL	0.7127	0.7679	$\log_{10}(1+\|AL\|)$
AU	0.7234	0.7661	$\log_{10}(1+\|AU\|)$
PCI	0.7795	0.8071	PCI
Kp	0.8453	0.8637	Kp
am	0.8437	0.8617	$\log_{10}(1+am)$
Dst	0.6047	0.6679	Dst
SYMH	0.6095	0.6700	SYMH
ASYH	0.6482	0.6893	ASYM
S_{rate}	0.6243	0.6317	S_{rate}
mP_e	0.7428	0.8371	$\log_{10}(0.01+mP_e)$
mP_i	0.8237	0.8464	$\log_{10}(0.01+mP_i)$
P_{ips}	0.6843	0.6918	P_{ips}
n_{ips}	0.6602	0.6774	$\log_{10}(n_{ips})$
F_{e130}	0.5087	0.5271	F_{e130}
$F_{e1.2}$	0.5423	0.6914	$F_{e1.2}$

variables s_j, and τ_j (with $\tau_j \leq 0$) are the lead times of the solar-wind variables with respect to the magnetospheric variable m(t). The eight lead times are optimized to produce the highest correlation between the left-hand side and right-hand side of expression (1). With 16 magnetospheric variables, 128 lead times are obtained. Note that with standardized variables, the size of the coefficients c_j have straightforward interpretation.

Vector-vector correlations are performed between a magnetospheric state vector $\underline{\mathbf{M}}(t)$ and a solar-wind state vector $\underline{\mathbf{S}}(t)$ using canonical correlation analysis (CCA) (Borovsky, 2014; Borovsky and Denton, 2018; Borovsky and Osmane, 2019). Nine of the magnetospheric variables from Table 1 are used to construct a 9-dimensional

Table 2
For the multivariate fits between each magnetospheric variable and the eight solar-wind variables the optimized solar-wind lead times appear as the top numbers and the magnitude of the coefficient appears as the second numbers; for the bivariate fits the optimized lead times appear as the third numbers and the magnitude of the bivariate correlation coefficient appears as the bottom numbers. An asterisk next to the lead time denotes a weak fit coefficient as described in the text.

	key	v_{sw}	n_{sw}	F10.7	$-B_z$	$f(M_A)$	θ_{clock}	θ_{Bn}	$\Delta B/B_{mag}$
AE	multi lead	0 h	0 h	0 h*	0 h	0 h	−1 h	−1 h*	0 h*
	multi coeff	1.00	0.55	0.12	0.43	0.36	0.70	0.13	0.10
	bivar lead	0 h	0 h*	0 h*	−1 h	−1 h	−1 h	−1 h*	−1 h*
	bivar corr	0.47	0.06	0.14	0.55	0.18	0.57	0.09	0.15
AL	multi lead	0 h	0 h	0 h*	−1 h	0 h	0 h	−1 h*	0 h*
	multi coeff	1.00	0.42	0.10	0.72	0.33	0.51	0.12	0.08
	bivar lead	0 h	0 h*	0 h*	−1 h	−1 h	−1 h	−1 h*	−1 h*
	bivar corr	0.44	0.11	0.12	0.54	0.16	0.55	0.07	0.13
AU	multi lead	0 h	0 h	0 h	0 h	0 h	−1 h	−1 h*	0 h*
	multi coeff	1.00	0.71	0.19	0.37	0.39	0.61	0.12	0.14
	bivar lead	0 h	−5 h*	0 h	−1 h	−2 h	−1 h	−1 h*	0 h
	bivar corr	0.404	0.04	0.17	0.45	0.18	0.48	0.11	0.16
PCI	multi lead	0 h	0 h	0 h	0 h	0 h	−1 h	−1 h	−1 h*
	multi coeff	1.00	0.62	0.17	0.77	0.48	0.47	0.20	0.00
	bivar lead	0 h	−1 h*	0 h	0 h	−1 h	0 h	−1 h*	0 h*
	bivar corr	0.37	0.03	0.16	0.59	0.22	0.51	0.12	0.07
Kp	multi lead	0 h	0 h	0 h*	−2 h	0 h	0 h	−2 h*	0 h*
	multi coeff	1.00	0.68	0.06	0.31	0.42	0.26	0.05	0.11
	bivar lead	0 h	−13 h*	0 h*	−1 h	0 h	−1 h	−1 h*	0 h
	bivar corr	0.57	0.06	0.15	0.37	0.23	0.34	0.07	0.19
am	multi lead	0 h	0 h	0 h*	−2 h	0 h	0 h	−2 h*	0 h*
	multi coeff	1.00	0.71	0.09	0.27	0.44	0.29	0.05	0.15
	bivar lead	0 h	−14 h*	0 h	−1 h	0 h	−1 h	−1 h*	0 h
	bivar corr	0.56	0.07	0.17	0.34	0.23	0.34	0.07	0.22
Dst	multi lead	−2 h	−9 h	−9 h*	−2 h	0 h	0 h	−5 h*	−5 h
	multi coeff	1.00	0.27	0.07	0.72	0.52	0.18	0.12	0.17
	bivar lead	−1 h	0 h	−19 h	−2 h	−1 h	−2 h	−12 h*	0 h*
	bivar corr	0.44	0.26	0.16	0.38	0.31	0.27	0.04	0.05
SYMH	multi lead	−1 h	−10 h	−11 h*	−2 h	0 h	−1 h	−6 h*	−4 h
	multi coeff	1.00	0.23	0.06	0.73	0.51	0.23	0.14	0.19
	bivar lead	−1 h	0 h	−7 h*	−1 h	0 h	−1 h	−9 h*	0 h*
	bivar corr	0.43	0.28	0.15	0.40	0.31	0.29	0.04	0.05
ASYH	multi lead	0 h	0 h	0 h*	−1 h	0 h	−1 h	−1 h*	−2 h*
	multi coeff	1.00	0.79	0.07	0.96	0.58	0.17	0.15	0.06
	bivar lead	0 h	−7 h*	0 h*	−1 h	−1 h	−1 h	−1 h*	0 h*
	bivar corr	0.32	0.07	0.14	0.44	0.26	0.31	0.12	0.02
S_{rate}	multi lead	0 h	0 h	0 h*	−2 h*	0 h	0 h	0 h*	0 h*
	multi coeff	1.00	0.44	0.05	0.15	0.25	0.22	0.05	0.11
	bivar lead	0 h	0 h*	0 h*	0 h	−11 h*	0 h	−6 h*	−1 h
	bivar corr	0.53	0.11	0.03	0.21	0.10	0.22	0.04	0.19
mP_e	multi lead	0 h	0 h	0 h*	−3 h	0 h	−1 h	−1 h*	0 h*
	multi coeff	1.00	0.57	0.01	0.40	0.36	0.63	0.13	0.08
	bivar lead	0 h	0 h*	0 h*	−1 h	−2 h*	−1 h	−1 h*	0 h*
	bivar corr	0.49	0.04	0.08	0.51	0.01	0.53	0.10	0.15
mP_i	multi lead	0 h	0 h	−1 h*	−3 h	0 h	−1 h	−2 h*	0 h*
	multi coeff	0.75	1.00	0.07	0.18	0.43	0.18	0.11	0.07
	bivar lead	0 h	−1 h	0 h*	−2 h	−3 h	−2 h	−1 h	0 h*
	bivar corr	0.23	0.43	0.13	0.25	0.18	0.23	0.21	0.14
P_{ips}	multi lead	0 h	−4 h	−6 h	−14 h*	−4 h	−7 h*	−4 h*	−4 h*
	multi coeff	0.56	1.00	0.25	0.14	0.54	0.13	0.04	0.14
	bivar lead	0 h*	−6 h	−7 h	−12 h*	−3 h	−9 h*	−4 h*	0 h*
	bivar corr	0.14	0.39	0.24	0.12	0.25	0.11	0.13	0.04
n_{ips}	multi lead	−4 h	−4 h	−6 h	−14 h*	−4 h	−6 h	−2 h*	−4 h
	multi coeff	0.57	1.00	0.29	0.13	0.57	0.17	0.04	0.17
	bivar lead	0 h*	−5 h	−7 h	−12 h*	−3 h	−9 h*	−4 h*	0 h*
	bivar corr	0.14	0.35	0.28	0.11	0.26	0.13	0.14	0.03
F_{e130}	multi lead	0 h	−12 h*	−1 h*	−1 h	−1 h*	−1 h	−1 h*	−3 h*
	multi coeff	1.00	0.09	0.11	0.28	0.06	0.19	0.06	0.03
	bivar lead	0 h	−1 h	−1 h*	−1 h	−15 h*	−1 h	−3 h*	−3 h*
	bivar corr	0.48	0.26	0.00	0.21	0.09	0.20	0.06	0.12
$F_{e1.2}$	multi lead	−59 h	−9 h	−9 h	−22 h	−9 h	−38 h	−22 h*	70 h*
	multi coeff	0.74	1.00	0.35	0.16	0.43	0.16	0.08	0.07
	bivar lead	−32 h	−11 h	−11 h	−36 h*	0 h	−37 h*	−15 h	−46 h
	bivar corr	0.57	0.51	0.16	0.09	0.17	0.09	0.16	0.17

magnetospheric state vector $\underline{\mathbf{M}}(t)$ and the eight solar-wind quantities used in multivariate correlations are used to construct an 8-dimensional solar-wind state vector $\underline{\mathbf{S}}(t)$. The CCA process yields a relation of the form

$$\begin{aligned} &C_1m_1(t+\tau_1) + C_2m_2(t+\tau_2) + C_3m_3(t+\tau_3) + C_4m_4(t+\tau_4) + C_5m_5(t+\tau_5) + C_6m_6(t+\tau_6) \\ &+ C_7m_7(t+\tau_7) + C_8m_8(t+\tau_8) + C_9m_9(t+\tau_9) \leftrightarrow c_1s_1(t) + c_2s_2(t) + c_3s_3(t) \\ &+ c_4s_4(t) + c_5s_5(t) + c_6s_6(t) + c_7s_7(t) + c_8s_8(t) \end{aligned} \quad (2)$$

where m_i are the magnetospheric variables, C_i are their numerical coefficients, and $\tau_i \geq 0$ are nine independent time lags of the magnetospheric variables from the time of the solar wind at Earth. An evolutionary algorithm (cf. Borovsky, 2017) is used to randomly vary the nine τ_i values to obtain the highest correlation coefficient between the left-hand side and right-hand side of expression (2), while the C_i and c_j coefficients at each evolutionary iteration are solved using canonical correlation analysis.

Bivariate correlations, multivariate correlations, and vector-vector correlations between the solar wind and the magnetosphere will yield some differences in the results, chiefly owing to the intercorrelations between the various solar-wind variables and the intercorrelations between the various magnetospheric variables. For example, in a bivariate correlation with a magnetospheric variable the solar-wind variable can carry information about other solar-wind variables (termed "confounding" (Robins, 1989; Frank, 2000)). In a multivariate correlation, two solar-wind variables can carry some of the same information and their individual importances in the correlation can therefore be reduced (related to "suppression" (Conger, 1974; Tzelgov and Henik, 1991)). In vector-vector correlations two magnetospheric variables can carry some of the same information and their individual importances in the correlation can therefore be reduced.

3. Single magnetospheric variables and the solar wind

Bivariate linear correlations and multivariate linear correlations are performed between magnetospheric variables and solar-wind variables.

The bivariate correlations between a single magnetospheric variable and a single solar-wind variable are performed with a lead time on the solar wind variable, and the lead time is adjusted in 1-hr increments until the maximum Pearson linear correlation R_{corr} is obtained. Those 128 optimized lead times are collected as the third number in each cell of Table 2 and the magnitude of the two-variable Pearson correlation coefficient is collected as the bottom number in each cell of Table 2.

In Fig. 1 the magnitude of the bivariate correlation coefficients $|R_{corr}|$ are plotted. Fig. 1a plots $|R_{corr}|$ for the high-latitude geomagnetic indices AE (red), AL (blue), AU (green), and PCI (dark red) in the functional forms listed in the final column of Table 1. The four high-latitude indices have very similar $|R_{corr}|$ patterns with the strongest correlations with v_{sw}, $-B_z$, and θ_{clock}.

In Fig. 1b the values of the bivariate correlation coefficients $|R_{corr}|$ are plotted for the convective indices Kp (red) and am (blue) and for the diamagnetic indices Dst (orange), SYMH (green), and ASYH (dark red). The $|R_{corr}|$ patterns for these five indices are similar. One noticeable difference is that Dst and SYMH have higher correlations with n_{sw} than the other three indices do. Another difference is that Kp and am are correlated most strongly with v_{sw}, with Dst and SYMH having a weaker correlation with v_{sw}, and ASYH having the weakest correlation with v_{sw}.

Fig. 1c plots the bivariate $|R_{corr}|$ values for the substorm occurrence rate Srate, and the electron precipitation mP_e and ion precipitation mP_i energy fluxes. Srate (red) has strongest correlation with v_{sw} with its other correlations considerably weaker. The electron precipitation mP_e (blue) has its strongest correlation with v_{sw}, $-B_z$, and θ_{clock}. The ion precipitation mP_i (green) has its strongest correlation with n_{sw}.

Fig. 1d plots the bivariate $|R_{corr}|$ values for the ion-plasma-sheet pressure P_{ips} and number density n_{ips}, for the substorm-injected electron flux F_{e130}, and for the outer-electron-radiation-belt flux $F_{e1.2}$. P_{ips} (red) and n_{ips} (blue) show very similar $|R_{corr}|$ patterns with the strongest correlations with n_{sw}. Note also that P_{ips} and n_{ips} have the highest F10.7 correlations in all of Fig. 1. F_{e130} (green) has its strongest correlation with v_{sw} and fairly weak correlations with the other solar-wind variables. The electron-radiation-belt flux $F_{e1.2}$ (dark red) is most-strongly correlated with v_{sw}, with its correlation with n_{sw} also high.

Multivariate linear correlation is performed between single magnetospheric variables and the set of 8 solar-wind variables with the 8 coefficients c_j of the solar-wind variables and the eight lead times τ_j all chosen to yield the largest Pearson linear correlation coefficient R_{corr} between the two sides of expression (1). For each magnetospheric variable the value of the Pearson linear correlation coefficient R_{corr} is listed in the second column of Table 1, the eight lead times τ_j of the solar-wind variables are listed as the upper values in Table 2, and the eight coefficients c_j of the solar-wind variables are plotted in Fig. 2 and listed as the second values in Table 1. Note again that the time-lag values can only be change by 1-hr increments in the 1991–2007 1-hr-resolution data set.

The first column of Table 1 lists the Pearson linear correlation coefficients for multivariate correlations between each magnetospheric variable and the set of eight solar-wind variables when all lead times are set to zero. The correlation coefficients without the lead times are high, but the correlation coefficients with the optimized lead times are factors of 1.01–1.27 times higher.

In Fig. 2 the eight coefficients of the eight solar-wind variables are plotted for each magnetospheric variable. The coefficients are normalized so that the largest of the eight coefficients has a magnitude of unity. For most of the magnetospheric variables the solar-wind velocity v_{sw} has the largest coefficient; for mP_i, n_{ips}, P_{ips}, and $F_{e1.2}$ the solar-wind number density n_{sw} has the largest coefficient. The largest coefficient represents the solar-wind quantity that has the strongest influence in the multivariate correlation.

Note in the panels of Fig. 2 that the areas under the curves are not indications of the strength of coupling of the magnetospheric variable to the solar wind: the proper measure of the coupling strength is the R_{corr} value in Table 1.

Fig. 2a plots the solar-wind-variable coefficients for the high-latitude geomagnetic indices AE (=AU-AL), AL, AU, and PCI. Two strong differences can be noted between AL (blue) and AU (green): the multivariate fit to AU depends more strongly on the solar-wind number density n_{sw} than does AL and AL depends more strongly on $-B_z$ than does AU. The multivariate fit to the polar cap index PCI (dark red) also has a strong dependence on $-B_z$. Note that the F10.7 coefficients for the high-latitude indices are larger than they are for most other magnetospheric quantities in Fig. 2; the high-latitude indices have modest dependencies on F10.7 whereas most other magnetospheric quantities do not.

Fig. 2b plots the solar-wind-variable coefficients for the convection indices Kp and am and the diamagnetic indices Dst, SYMH, and ASYH. In Fig. 2b ASYH (dark red) behaves similar to SYMH and Dst (green and orange) with the exception that the multivariate fit to ASYH is more strongly dependent on n_{sw} and has a reversed dependence on θ_{clock}. The multivariate fit to the convection indices Kp (red) and am (blue) have

strong dependences on v_{sw}, $-B_z$, and $f(M_A)$.

Fig. 2c plots the solar-wind-variable coefficients for the substorm occurrence rate S_{rate} (red) and the hemispheric power of electron precipitation mP_e (blue) and ion precipitation mP_i (green). Comparing the ion and electron precipitation coefficients, the multivariate fit to mP_i depends much more strongly on n_{sw} than does mP_e and the multivariate fit to mP_e depends much more strongly on θ_{clock} than does mP_i. Note in Fig. 2c that the substorm occurrence rate S_{rate} is dominated almost entirely by the solar-wind velocity v_{sw} with the magnitude of all other solar-wind coefficients being modest.

Fig. 2d plots the multivariate fit coefficients for the particle indices n_{ips} (blue) and P_{ips} (red) for the ion plasma sheet, F_{e130} (green) for the substorm-injected electrons, and $F_{e1.2}$ (dark red) for the outer electron radiation belt. Note the strong dependences of n_{ips} and P_{ips} on the solar-wind density n_{sw}, with secondary dependences on the solar-wind velocity v_{sw} and on $f(M_A)$. The Mach-number function $f(M_A)$ describes, in part, the number density of the magnetosheath (Borovsky, 2008; Borovsky and Birn, 2014), as does n_{sw}. The multivariate fits to the ion plasma sheet density n_{ips} and pressure P_{ips} have weak dependencies on $-B_z$ and θ_{clock}. Note that unlike most magnetospheric quantities in Fig. 2, n_{ips}, P_{ips}, and $F_{e1.2}$ have modest dependencies on F10.7. In Fig. 2d the multivariate fit to the substorm-injected electron population F_{e130} (green) depends almost exclusively on the solar-wind velocity v_{sw}; this is similar to the substorm occurrence rate S_{rate} (red) in Fig. 2c, which has a singular dependency on v_{sw}. The multivariate fit to the outer electron radiation belt flux index $F_{e1.2}$ (dark red) has a strong negative connection to n_{sw} and a strong positive connection to v_{sw}; these two simultaneous connections are well known (Balikhin et al., 2011; Boynton et al., 2013; Wing et al., 2016). In the multivariate fit to $F_{e1.2}$ the connection is stronger to n_{sw} than it is to v_{sw}, but the situation is more complicated: Borovsky (2017) pointed out that time-integrals of solar-wind variables have higher correlations with $F_{e1.2}$ than do time-lagged solar-wind variables and when time integration is accounted for the solar-wind velocity has a stronger influence on $F_{e1.2}$ than does the solar wind density. In Fig. 1d the bivariate correlation coefficient $|R_{corr}|$ of $F_{e1.2}$ is higher with v_{sw} than it is with n_{sw}. The negative connection of $F_{e1.2}$ to n_{sw} represents loss of radiation belt electrons connected with increases in the solar wind number density and the positive connection of $F_{e1.2}$ to v_{sw} represents energization of the radiation-belt electrons when the solar-wind velocity is high.

The optimized lead times for the eight solar-wind variables (columns) are listed in Table 2 for each of the magnetospheric variables (rows). The upper number is the lead time obtained with the multivariate fits, the second number is the multivariate normalized coefficient (i.e. those plotted in Fig. 2), the third number is the lead time obtained from the bivariate correlations, and the bottom number is the bivariate correlation coefficient. The multivariate lead times on solar-wind variables that have weak coefficients are marked with an asterisk, where "weak" means the magnitude of the coefficient is 15% or less of the magnitude of the largest coefficient; bivariate lead times are marked with an asterisk if the bivariate correlation coefficient $|R_{corr}|$ is ≤ 0.15.

The first four rows of Table 2 are the high-latitude geomagnetic indices AE, AL, AU, and PCI; in the 1-hr resolution data sets these high-latitude indices show little lag from the solar wind variables. The multivariate time lags of 1 h from the solar wind θ_{clock} value for AE, AU, and PCI is probably significant as is the 1-hr lag of AL with respect to the value of $-B_z$; the significance of the multivariate lag for each solar-wind variable is gauged by the magnitude of the solar-wind-variable coefficient (second value in Table 2). The lags of AE, AU, and PCI with θ_{Bn} and $\Delta B/B_{mag}$ are not significant since the coefficients of the high-latitude indices with θ_{Bn} and $\Delta B/B_{mag}$ are quite small (cf. Fig. 2a). The time lags obtained with the two methods (bivariate and multivariate) are more-or-less in agreement for these high-latitude indices.

In the 5th and 6th rows of Table 2 the multivariate correlations for the convective indices Kp and am show 2-hr lags with respect to both $-B_z$ and θ_{Bn}, neither of which has strong significance since the coefficients of

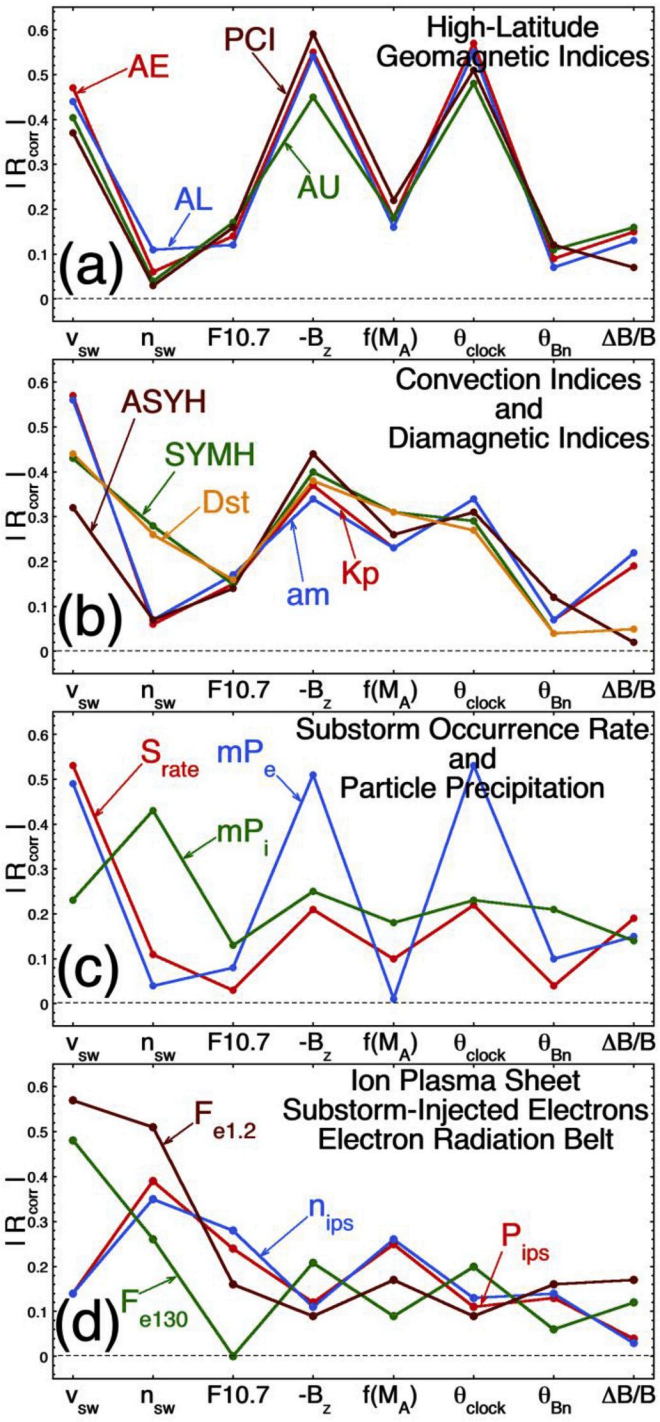

Fig. 1. For bivariate linear correlations between single magnetospheric variable and single solar-wind variable with an optimized lead time, the magnitude of the correlation coefficient $|R_{corr}|$ is plotted. The sixteen curves for 16 magnetospheric variables are grouped into (a) high-latitude geomagnetic indices, (b) convection and diamagnetic indices, (c) electron and ion precipitation and the substorm occurrence rate, and (d) the properties of the ion plasma sheet, substorm-injected electrons, and the electron radiation belt. As noted in Section 2 the standard errors on the correlation coefficients are 0.003 or less.

$-B_z$ and θ_{Bn} are modest for these convective indices (cf. Fig. 2b). The bivariate correlations show 13–14 h lags between these indices and n_{sw}, but the correlation is extremely weak and those lag values are not significant.

In the 7th and 8th rows of Table 2 the multivariate correlations for the two diamagnetic indices Dst and SYMH show similar lags with respect to the solar wind with lags of 1–2 h from the value of v_{sw} (significant), 9–10 h from n_{sw} (modestly significant), 9–11 h from F10.7 (not significant), 2 h from $-B_z$ (significant), 0–1 h from θ_{clock} (modestly significant), 5–6 h from θ_{Bn} (modestly significant), and 4–5 h from the value of $\Delta B/B_{mag}$ (modestly significant), where significance here is judged by the magnitude of the solar-wind-variable coefficients plotted in Fig. 2b. A noticeable disagreement between the bivariate and multivariate results is the time lag between n_{sw} and the indices Dst and SYMH: the bivariate method yields a time lag of 0 h and the multivariate method yields lags of 9–10 h. The bivariate correlation coefficient has a distinct peak at 0-hr lag, but in the evolutionary scheme with multivariate fits if the lead time on n_{sw} is zeroed it repeatedly evolves away from zero. Almost certainly the difference between the answers from the two methods is caused by the intercorrelations of solar-wind variables in the multivariate fitting, most likely the strong, lagged intercorrelation between v_{sw} and n_{sw} (cf. Wing et al., 2016; Borovsky, 2018).

In the 9th row the multivariate time lags of ASYH are 1 h with respect to $-B_z$ (significant), 1 h from θ_{clock} (less significant) and from θ_{Bn} (less significant), and 2 h from $\Delta B/B_{mag}$ (not significant). Where the lag values are significant (no asterisks), the bivariate method agrees with the multivariate method. The disagreement between the lags of ASYM with respect to n_{sw} has a very low correlation coefficient and is not significant.

In the 10th row of Table 2 the substorm occurrence rate S_{rate} shows a 2 h lag with respect to $-B_z$ in the multivariate lags, which is not really significant since the coefficient from the value of $-B_z$ is only 0.153 in Fig. 2c. There is no disagreement from the bivariate time lags for S_{rate} where there is significance (no asterisk).

In the 11th and 12th rows the hemispheric power of particle precipitation mP_e and mP_i show multivariate lags of 0–1 h with respect to F10.7 (not significant), 3 h from $-B_z$ (more significant for mP_e than for mP_i), 1 h from θ_{clock} (more significant for mP_e than for mP_i), and 1–2 h from the value of θ_{Bn} (very modest significance), as judged by the coefficient magnitudes. Where significant, the time lags from the bivariate method are similar to the multivariate lags: the mP_i to $f(M_A)$ lag of 3 h is close to insignificant with a correlation coefficient of only 0.18.

The 13th and 14th rows of Table 2 display the solar-wind multivariate lead times with respect to the ion-plasma-sheet properties: P_{ips} and n_{ips} show 4 h lags from n_{sw} (significant), 0–4 h lags from v_{sw} (significant), 4 h lags from $f(M_A)$ (significant), 6 h lags from F10.7 (modestly significant), and lags with respect to θ_{clock}, θ_{Bn}, and $\Delta B/B_{mag}$ that are of low significance. Where significant, the bivariate time lags agree within 1 h of the multivariate time lags.

Row 15 of Table 1 displays the solar-wind multivariate lead times for the substorm-injected electron flux F_{e130}, which shows a 12-hr lag time with respect to the value of n_{sw} (not significant), 1-hr time lags from F10.7, $f(M_A)$, and θ_{Bn} (all of which are not significant), a 3-hr time lag from $\Delta B/B_{mag}$ (not significant), and 1-hr time lags from $-B_z$ and from θ_{clock} (both of which are modestly significant), judged by the magnitudes of the multivariate coefficients. Where they are significant, the bivariate time lags for F_{e130} agree with the multivariate time lags to within 1 h.

The final row of Table 2 displays the optimized solar-wind lead times for the electron radiation belt 1.2-MeV flux $F_{e1.2}$, which shows multivariate lags of −59 h with respect to v_{sw} (significant), 9 h from n_{sw} (significant), 9 h from F10.7 (modestly significant), 22 h from $-B_z$ (not significant), and 9 h from $f(M_A)$ (modestly significant), 38 h from θ_{clock} (not significant), 22 h from θ_{Bn} (not significant), and 70 h from $\Delta B/B_{mag}$, with significance judged by the magnitude of the multivariate coefficients. The lag time of 32 h between Fe1.2 and v_{sw} found by the bivariate method is about half of the large lag of 59 h time found by the multivariate method. The bivariate lag times from n_{sw} and F10.7 are 11 h instead of 9 h. The bivariate lag time is 0 h for $f(M_A)$ while the multivariate method finds 9 h, however the bivariate value has a very weak correlation coefficient (0.17). Other $F_{e1.2}$ lags are not significant.

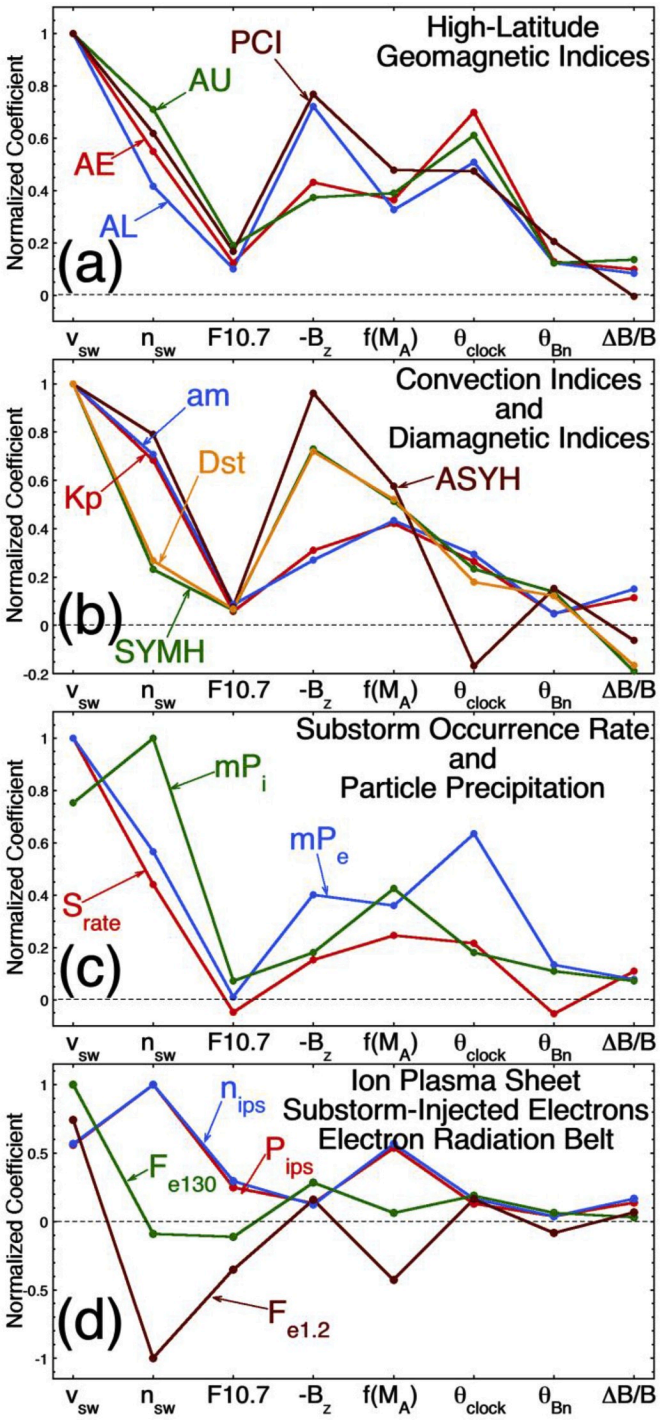

Fig. 2. For multivariate linear correlations between a single magnetospheric variable and eight solar-wind variables with eight optimized lead times, the fit coefficients of the solar-wind variables are plotted. The sixteen curves for 16 magnetospheric variables are grouped into (a) high-latitude geomagnetic indices, (b) convection and diamagnetic indices, (c) electron and ion precipitation and the substorm occurrence rate, and (d) the properties of the ion plasma sheet, substorm-injected electrons, and the electron radiation belt.

4. State-vector correlations

The correlation between the time-dependent solar-wind state vector $\underline{\mathbf{S}}(t)$ and the time-dependent magnetospheric state vector $\underline{\mathbf{M}}(t)$ will describe a global mode of reaction of the magnetosphere to the solar wind. To produce the solar-wind state vector $\underline{\mathbf{S}}(t)$, the eight solar-wind

Table 3
In the vector-vector correlations between the solar-wind state vector and the magnetospheric state vector, the nine optimized time lags of the magnetospheric variables are listed.

Quantity	Lag
AL	1 h
AU	2 h
PCI	0 h
am	0 h
ASYH	1 h
mP_e	0 h
mP_i	1 h
P_{ips}	0 h
F_{e130}	0 h

quantities used in the multivariate correlations of Section 3 are used. To produce the magnetospheric state vector $\underline{\mathbf{M}}(t)$, nine magnetospheric quantities from Table 1 are chosen. Where variables carry much the same information (e.g. (a) Kp and am, (b) P_{ips} and n_{ips}, (c) SYMH and Dst, and (d) AE = AU-AL and AU and AL) one variable is not used. The nine variables listed in Table 3 are the ones used.

In the vector-vector correlations, the nine magnetospheric variables are time lagged from the solar wind at Earth, with the nine independent time lags optimized to produce the highest Pearson linear correlation coefficient between the solar-wind state vector and the magnetospheric state vector. The result is the relation

$$\begin{aligned} &0.25104\ \log_{10}(1+|\mathrm{AL}|) + 0.28197\ \log_{10}(1+|\mathrm{AU}|) + 0.64556\ \mathrm{PCI} \\ &+ 1.0000\ \log_{10}(\mathrm{am}) + 0.23408\ \mathrm{ASYH} \\ &- 0.26899\ \log_{10}(0.01 + \mathrm{mP_e}) + 89827\ \log_{10}(0.01 + \mathrm{mPi}) \\ &+ 0.33487\ \mathrm{P_{ips}} - 0.03221\ \mathrm{F_{e130}} \leftrightarrow 1.0000\ \log_{10}(\mathrm{v_{sw}}) \\ &+ 0.95333\ \log_{10}(\mathrm{n_{sw}}) + 0.13446\ \log_{10}(\mathrm{F10.7}) + 0.35924\ (-B_z) \\ &+ 0.53072\ \mathrm{f(M_A)} + 0.21455\ \sin^2(\theta\mathrm{clock}/2) + 0.087224\ \theta_{\mathrm{Bn}} \\ &+ 0.092932\ \left(0.1 + \Delta\mathrm{B}/\mathrm{B_{mag}}\right) \end{aligned} \tag{3}$$

The reader is reminded that all variables in expression (3) are in standardized form with a mean value of zero and a standard deviation of unity. The vector-vector time lags on the magnetospheric variables are optimized to maximize the correlation between the global reaction mode of the magnetosphere and the solar wind. The optimized time time lags on the nine magnetospheric variables of expression (3) are entered into Table 3 and the coefficients of expression (3) are plotted in Fig. 3. The Pearson linear correlation coefficient between the left-hand side and right-hand side of expression (3) is $R_{corr} = 0.9031$. If the vector-vector correlation is performed without allowing for time lags, the correlation coefficient is $R_{corr} = 0.8946$. An increase in R_{corr} from 0.8964 to 0.9031 represents a decrease of the unaccounted for variance $1\text{-}R^2_{corr}$ from 0.1998 to 0.1844, which is a decrease by 7.7%.

The coefficients of the solar-wind variables driving the global magnetospheric mode are plotted in Fig. 3a for the case of no time lags (red curve with hollow points) and for the case of optimized time lags (blue curve with solid points). The global mode is strongly driven by the solar-wind velocity v_{sw} and density n_{sw}, and somewhat by the Mach number function $f(M_A)$. Other solar-wind quantities are not as important. Comparing the two curves in Fig. 3a, when the time lags are allowed the roles of $-B_z$ and θ_{clock} increase and the role of n_{sw} decreases.

The coefficients of the magnetospheric variables describing the global reaction mode are plotted in Fig. 3b, red-hollow for no time lags and blue-solid for optimized time lags. The mode is dominantly described by am, PCI, and mP_i with F_{e130} playing almost no role. (F_{e130} plays roles in secondary modes of reaction.) Comparing the two curves in Fig. 3b, it is seen that the coefficients describing the global mode do

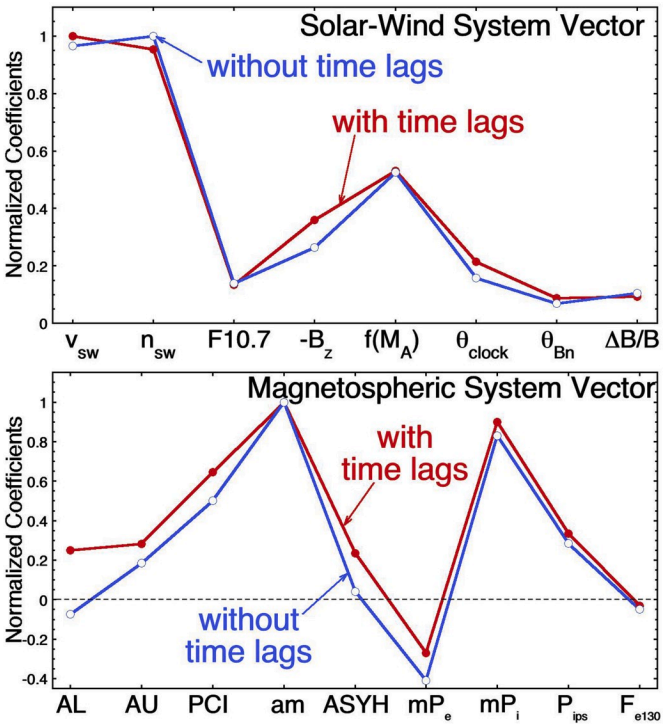

Fig. 3. For vector-vector correlations between a 9-dimensional magnetospheric state vector $\underline{\mathbf{M}}(t)$ and an 8-dimensional solar-wind state vector $\underline{\mathbf{S}}(t)$ the numerical coefficients for the 8 variables of the solar-wind vector are plotted in panel (a) and the numerical coefficients for the 9 variables of the magnetosphere are plotted in panel (b). The red curves with hollow points are for the case of no time lags and the blue curves with solid points are for the case of 9 optimized time lags on the 9 magnetospheric variables.

not change strongly when time lags are allowed: the roles of almost all variables increase slightly while the role of mP_e decreases.

The optimized time lags of the magnetospheric variables from the solar wind are listed in Table 3. 1-hr lags are found for AL, ASYH, and mP_i and a 2-hr lag is found for AU. The lag for mP_i is probably significant since the coefficient for mP_i is large in Fig. 3b and the other lags have weaker significance since the coefficients are weaker. Comparing the magnetospheric lag times of Table 3 to the solar-wind lead times of Table 2 shows no obvious connection.

If lead times on the eight solar-wind variables are allowed in addition to the lag times on the nine magnetospheric variables, the same pattern of magnetospheric lag times is found: 1-hr lags are found for AL, ASYH, and mP_i and a 2-hr lag is found for AU. There is almost no increase in the correlation, and the optimized lead times on the solar-wind variables are -2 h on θ_{clock} and -1 h on $f(M_A)$.

5. Overview, discussion, and the future

The time lags between magnetospheric variables and solar-wind variables found in the multivariate correlations and bivariate correlations of Section 3 are collected in Table 2. Lags on weak variables are marked with an asterisk in Table 2. It is reasonable to consider time lags with asterisks in Table 2 as not significant. In Table 2 some general patterns of the time lags can be seen. The high-latitude and convection geomagnetic indices AE, AL, AU, PCI, Kp, and am exhibit 1–2 h time lags with respect to a few solar-wind variables, typically $-B_z$, θ_{clock}, and θ_{Bn}, which are three solar-wind variables with short autocorrelation times. The diamagnetic index ASYH has similar time lags. The diamagnetic indices SYMH and Dst show different lags: 1–2 h with respect to the solar-wind velocity v_{sw} and 9–10 h with respect to the solar-wind number density n_{sw} and they show shorter time lags with respect to

-B_z and θ_{clock}. The substorm occurrence rate S_{rate} has lags similar to those of the convection indices: 2 h with respect to B_z. The particle precipitation rates mP_e and mP_i have lags of 3 h on B_z and 1 h with respect to θ_{clock}. The geosynchronous-orbit ion plasma sheet pressure P_{ips} and density n_{ips} show 0–4 h lags with respect to v_{sw}, 4 h lags with respect to n_{sw}, 7-hr lags with respect to F10.7 and 4-hr lags with respect to θ_{clock}; F10.7 is a 24-hr resolution index with a very long autocorrelation time and so its lag of a fraction of a day is probably not meaningful. The substorm-injected electron flux F_{e130} depends almost exclusively on v_{sw}, which shows no time lag; F_{e130} does have lags with respect to -B_z and θ_{clock} but they are weaker variables. The electron radiation belt flux $F_{e1.2}$ shows the familiar long lag (32–59 h) with respect to the solar-wind velocity v_{sw} (with a positive correlation) and a much shorter lag (9–11 h) with respect to the solar-wind number density n_{sw} (with an anticorrelation). $F_{e1.2}$ also shows a multivariate 9-hr lag on $f(M_A)$, which describes in part the number density of the magnetosheath with respect to the number density of the solar wind (Borovsky, 2008; Borovsky and Birn, 2014).

In Table 4 the influences of the eight solar-wind variables in the multivariate and bivariate fits of Section 3 are compared. The first column of Table 4 is the average magnitude of the normalized coefficients for the 16 multivariate correlations plotted in Fig. 2. For each of the 16 magnetospheric variables the magnitudes of the eight coefficients are ranked from 1 to 8: in the second column of Table 4 the average of the 16 rankings is listed. In the third column of Table 4 the average of the bivariate correlation coefficients from Table 2 are listed for the eight variables. The second number in each column of Table 4 is the ranking of the number in that column. By these three measures the solar-wind velocity v_{sw} is the dominant solar-wind variable in the solar-wind/magnetosphere correlations having the largest average magnitude of its coefficients, having the highest average rank of its coefficients, and having the highest average bivariate correlation coefficient. The second most dominant solar-wind variable in the multivariate correlations (first and second columns) is the number density n_{sw}, but in the bivariate correlations -B_z (third column) comes in second while n_{sw} comes in fifth. The multivariate fitting may be giving n_{sw} large coefficients because of unique information that it carries relative to other solar-wind variables. Note in the bivariate correlations the correlation coefficients of -B_z and θ_{clock} rank 2 and 3 while in the multivariate rankings (first and second columns) they rank 3 and 5; since these two variables carry similar information about the orientation of the solar-wind magnetic field, the multivariate fits simultaneously use both variables and give them each lower coefficients. According to all three columns of Table 4, the variables F10.7, $\Delta B/B_{mag}$, and θ_{Bn} are the least influential in the solar-wind correlations with the magnetosphere. Of course, for individual magnetospheric variables the ranking of the influence of the eight solar-wind variables differs from the average ranking seen in Table 4.

In the multivariate correlations, the variable $\Delta B/B_{mag}$ has a weak influence. However, previous studies have demonstrated that $\Delta B/B_{mag}$ has an effect on geomagnetic activity (Borovsky and Funsten, 2003; Borovsky, 2006; D'Amicis et al., 2007, 2010; Osmane et al., 2015). If solar-wind/magnetosphere data is sorted in a fashion to keep the rate of dayside reconnection within a fixed range of values, then $\Delta B/B_{mag}$ is clearly seen to have a positive correlation with geomagnetic activity (Borovsky and Steinberg, 2006), but the effect is small, and not understood.

Using vector-vector correlations in Section 4, the allowance for multiple magnetospheric time lags with respect to the solar wind (and also allowance for multiple solar-wind lead times with respect to the magnetosphere) yields larger correlation coefficients over non-lag and non-lead vector-vector correlations. However, the physical meaning of the optimized time lags is difficult to determine and those vector-vector lags are not obviously related to the more-interpretable bivariate and multivariate time lags.

It is not straightforward to interpret the physical meaning of these time lags that are optimized to yield the highest correlation coefficients between the solar wind and the magnetosphere. One complication is that differences are found between lag values optimizing single solar-wind variables in bivariate correlations (where the interpretation is more clear) versus optimizing the set of lags in the set of solar-wind variables in multivariate fits (where the correlation is much higher). It is unambiguous to say that these optimized lags are the time lags in the correlations in the data sets: attributing the lags to physical cause, to timescales of physical processes, or to transport times is another matter. The ubiquitous intercorrelations between solar-wind variables with various lag-lead times (Wing et al., 2016; Borovsky, 2018) is perhaps the biggest hindrance to determining the importance of a correlation and the physical interpretation of its lag. A secondary complication is that the calculated lag times can be uncertain. When correlations are strong the correlation lag times are clear to obtain: when correlations are weak variations the value of a lag time do not strongly affect correlation coefficients and the values of the optimized lags tend to drift. Similarly, for solar-wind quantities with long autocorrelation times (such as v_{sw} and F10.7) the values of the calculated lags can drift without strong impact on correlation coefficients.

Table 4
For the 16 multivariate correlations for the 16 magnetospheric variables, the average of the 16 coefficients of each of eight solar-wind variables is listed in the first column and the average rank of the magnitude of the 16 coefficients is listed in the second column. The average of the 16 bivariate correlation coefficients for each of the eight solar-wind variables is listed in the final column. The second number in each column is the rank of that row in that column.

	Mean Multivariate Coefficient Magnitude	Mean Mutivariate Rank	Mean Bivariate Correlation Coefficient
v_{sw}	0.914 1st	1.3 1st	0.412 1st
n_{sw}	0.629 2nd	2.6 2nd	0.192 5th
F10.7	0.129 6th	6.5 6th	0.142 6th
-B_z	0.420 3rd	3.9 4th	0.347 2nd
$f(M_A)$	0.416 4th	3.8 3rd	0.196 4th
θ_{clock}	0.320 5th	4.2 5th	0.323 3rd
θ_{Bn}	0.101 8th	6.9 7th,8th	0.098 8th
$\Delta B/B_{mag}$	0.104 7th	6.9 7th,8th	0.118 7th

Expanding this work in the future with additional (and new) magnetospheric and ionospheric measures could provide more information. Possible measurements to utilize are the polar-cap size, the intensity of auroral kilometric radiation, the total radiation belt electron content, ULF amplitudes (e.g. Kozyreva et al., 2007; Romanova et al., 2007; Borovsky and Denton, 2014), Plasma-wave intensities, various ionospheric total electron content measures, the Schumann resonance intensity (e.g. Fullekrug et al., 2002; Toledo-Redondo et al., 2016), and ionospheric ion-outflow rates (e.g. Welling et al., 2015). Investigating the optimization of time lags using information theory (e.g. Johnson et al., 2018; Wing and Johnson, 2019) rather than correlation might provide new interpretation of the causal lags between solar-wind properties and magnetospheric reactions.

Acknowledgements

The author thanks Mick Denton for useful conversations and programming assistance. This work was supported by the NASA Heliophysics LWS TRT program via grant NNX14AN90G, by the NSF GEM Program via award AGS-1502947, by the NASA Heliophysics Guest Investigator Program via grant NNX17AB71G, by the NSF SHINE program via award AGS-1723416.

References

Arnoldy, R.L., 1971. Signature in the interplanetary medium for substorms. J. Geophys. Res. 76, 5189.

Balikhin, M.A., Boynton, R.J., Walker, S.N., Borovsky, J.E., Billings, S.A., Wei, H.L., 2011. Using the NARMAX approach to model the evolution of energetic electrons fluxes at geostationary orbit. Geophys. Res. Lett. 38, L181051.
Bendat, J.S., Piersol, A.G., 1971. Random Data: Analysis and Measurement Procedures, 4.8.1. John Wiley, New York. Sect.
Beyer, W.H., 1966. Handbook of Tables for Probability and Statistics. Sect. IX. Chemical Rubber Company, Cleveland, Ohio.
Borovsky, J.E., 2006. Eddy viscosity and flow properties of the solar wind: Co-rotating interaction regions, coronal-mass-ejection sheaths, and solar-wind/magnetosphere coupling. Phys. Plasmas 13, 056505.
Borovsky, J.E., 2008. The rudiments of a theory of solar-wind/magnetosphere coupling derived from first principles. J. Geophys. Res. 113, A08228.
Borovsky, J.E., 2014. Canonical correlation analysis of the combined solar-wind and geomagnetic-index data sets. J. Geophys. Res. 119, 5364.
Borovsky, J.E., 2017. Time-integral correlations of multiple variables with the relativistic-electron flux at geosynchronous orbit: the strong roles of the substorm-injected electrons and the ion plasma sheet. J. Geophys. Res. 122, 11961.
Borovsky, J.E., 2018. On the origin of the intercorrelations between solar-wind variables. J. Geophys. Res. 123, 20.
Borovsky, J.E., Birn, J., 2014. The solar-wind electric field does not control the dayside reconnection rate. J. Geophys. Res. 119, 751.
Borovsky, J.E., Denton, M.H., 2014. Exploring the cross-correlations and autocorrelations of the ULF indices and incorporating the ULF indices into the systems science of the solar-wind-driven magnetosphere. J. Geophys. Res. 119, 4307.
Borovsky, J.E., Denton, M.H., 2018. Exploration of a composite index to describe magnetospheric activity: reduction of the magnetospheric state vector to a single scalar. J. Geophys. Res. 123, 7384.
Borovsky, J.E., Funsten, H.O., 2003. Role of solar wind turbulence in the coupling of the solar wind to the earth's magnetosphere. J. Geophys. Res. 108, 1246.
Borovsky, J.E., Osmane, A., 2019. Compacting the description of a time-dependent multivariable system and its time-dependent multivariable driver by reducing the system and driver state vectors to aggregate scalars: the earth's solar-wind-driven magnetosphere. Nonlinear Process Geophys. 26, 429.
Borovsky, J.E., Steinberg, J.T., 2006. The freestream turbulence effect in solar-wind/magnetosphere coupling: analysis through the solar cycle and for various types of solar wind. Geophys. Monogr. 167, 59.
Borovsky, J.E., Valdivia, J.A., 2018. The Earth's magnetosphere: a systems science overview and assessment. Surv. Geophys. 39, 817.
Borovsky, J.E., Yakymenko, K., 2017. Systems science of the magnetosphere: creating indices of substorm activity, of the substorm-injected electron population, and of the electron radiation belt. J. Geophys. Res. 122, 10012.
Borovsky, J.E., Thomsen, M.F., Elphic, R.C., 1998. The driving of the plasma sheet by the solar wind. J. Geophys. Res. 103, 17617.
Boynton, R.J., Balikhin, M.A., Billings, S.A., Reeves, G.D., Ganushkina, N., Gadalin, M., Amariutei, O.A., Borovsky, J.E., Walker, S.N., 2013. The analysis of electron fluxes at geosynchronous orbit employing a NARMAX approach. J. Geophys. Res. 118, 1500.
Conger, A.J., 1974. A revised definition for suppressor variables: a guide to their identification and interpretation. Educ. Psychol. Meas. 34, 35.
D'Amicis, R., Bruno, R., Bavassano, B., 2007. Is geomagnetic activity driven by solar wind turbulence? Geophys. Res. Lett. 34, L05108.
D'Amicis, R., Bruno, R., Bavassano, B., 2010. Geomagnetic activity driven by solar wind turbulence. Adv. Space Res. 46, 514.
Davis, T.N., Sugiura, M., 1966. Auroral electrojet activity index AE and its Universal Time variations. J. Geophys. Res. 71, 785.
Denton, M.H., Borovsky, J.E., 2009. The superdense plasma sheet in the magnetosphere during high-speed-steam-driven storms: plasma transport timescales. J. Atmos. Sol. Terr. Phys. 71, 1045.
Emery, B.A., Coumans, V., Evans, D.S., Germany, G.A., Greer, M.S., Holeman, E., Kadinsky-Cade, K., Rich, F.J., Xu, W., 2008. Seasonal, Kp, solar wind, and solar flux variations in long-term single-pass satellite estimates of electron and ion auroral hemispheric power. J. Geophys. Res. 113, A06311.
Emery, B.A., Richardson, I.G., Evans, D.S., Rich, F.J., 2009. Solar wind structure sources and periodicities of auroral electron power over three solar cycles. J. Atmos. Sol. Terr. Phys. 71, 1157.
Frank, K.A., 2000. Impact of confounding variable on a regression coefficient. Socio. Methods Res. 29, 147.
Fullekrug, M., Fraser-Smith, A.C., Schlegel, K., 2002. Global ionospheric D-layer height monitoring. Europhys. Lett. 59, 629.
Iyemori, T., Maeda, H., Kamei, T., 1979. Impulse response of geomagnetic indices to interplanetary magnetic field. J. Geomagn. Geoelectr. 31, 1.
Johnson, J.R., Wing, S., Camporeale, E., 2018. Transfer entropy and cumulant-based cost as measures of nonlinear causal relationships in space plasmas: applications to D_{st}. Ann. Geophys. 36, 945.
Katus, R.M., Liemohn, M.W., 2013. Similarities and differences in low- to middle-latitude geomagnetic indices. J. Geophys. Res. 118, 5149.
King, J.H., Papitashvili, N.E., 2005. Solar wind spatial scales in and comparisons of hourly Wind and ACE plasma and magnetic field data. J. Geophys. Res. 110, 2104.
Kozyreva, O., Pilipenko, V., Engebretson, M.J., Yumoto, K., Watermann, J., Romanova, N., 2007. In search of a new ULF wave index: comparison of Pc5 power with dynamics of geostationary relativistic electrons. Planet. Space Sci. 55, 755.
Matzka, J., Stolle, C., Kervalishvili, G., Rauberg, J., Yamazaki, Y., 2019. The Hp Geomagnetic Index Test Dataset 2003, 2004, 2005 and 2017. GFZ Data Services org/10.5880/GFZ.2.3.2019.002.
Newell, P.T., Sotirelis, T., Liou, K., Meng, C.I., Rich, F.J., 2007. A nearly universal solar wind-magnetosphere coupling function inferred from 10 magnetospheric state variables. J. Geophys. Res. 112, A01206.
Osmane, A., Dimmock, A.P., Naderpour, R., Pulkkinen, T.I., Nykyri, K., 2015. The impact of solar wind ULF Bz fluctuations on geomagnetic activity for viscous timescales during strongly northward and southward IMF. J. Geophys. Res. 120, 9307.
Robins, J., 1989. The control of confounding by intermediate variables. Stat. Med. 8, 679.
Romanova, N., Plipenko, V., Crosby, N., Khabarova, O., 2007. ULF wave index and its possible applications in space physics. Bulg. J. Phys. 34, 136.
Smith, J.P., Thomsen, M.F., Borovsky, J.E., Collier, M., 1999. Solar wind density as a driver for the ring current in mild storms. Geophys. Res. Lett. 26, 1797.
Thomsen, M.F., 2004. Why Kp is such a good measure of magnetospheric convection. Space Weath 2, S11044.
Toledo-Redondo, S., Salinas, A., Fornieles, J., Porti, J., Lichtenberger, H.I.M., 2016. Full 2-D TLM simulations of the Earth-ionosphere cavity: effect of conductivity on the Schumann resonances. J. Geophys. Res. 121, 5579.
Troshichev, O.A., Andrezen, V.G., Vennerstrøm, S., Friis-Christensen, E., 1988. Magnetic activity in the polar cap – A new index. Planet. Space Sci. 11, 1095.
Tzelgov, J., Henik, A., 1991. Suppression situations in psychological research: definitions, implications, and applications. Psychol. Bull. 109, 524.
Weimer, D.R., King, J.H., 2008. Improved calculations of IMF phase-front angles and propagation time delays. J. Geophys. Res. 113, A01105.
Welling, D.T., Andre, M., Dandouras, I., Delcourt, D., Fazakerley, A., Fontaine, D., Foster, J., Ilie, R., Kistler, L., Lee, J.H., Liemohn, M.W., Slavin, J.A., Wang, C.-P., Wiltberger, M., Yau, A., 2015. The Earth: plasma sources, losses, and transport processes. Space Sci. Rev. 192, 145.
Wing, S., Johnson, J.R., 2019. Applications of information theory in solar and space physics. Entropy 21, 140.
Wing, S., Johnson, J.R., Camporeale, E., Reeves, G.D., 2016. Information theoretical approach to discovering solar wind drivers of the outer radiation belt. J. Geophys. Res. 121, 9378.